

## 1                   Circular RNA Vaccines against SARS-CoV-2 and Emerging Variants

2   **Liang Qu<sup>1\*</sup>, Zongyi Yi<sup>1,2\*</sup>, Yong Shen<sup>1,2</sup>, Yiyuan Xu<sup>1</sup>, Zeguang Wu<sup>1</sup>, Huixian Tang<sup>1</sup>, Xia**  
3 **Xiao<sup>3</sup>, Xiaojing Dong<sup>3</sup>, Li Guo<sup>3</sup>, Ayijiang Yisimayi<sup>4</sup>, Yunlong Cao<sup>4</sup>, Zhuo Zhou<sup>1</sup>, Jianwei**  
4 **Wang<sup>3</sup>, Xiaoliang Sunney Xie<sup>4</sup>, Wensheng Wei<sup>1†</sup>**

5   <sup>1</sup>Biomedical Pioneering Innovation Center, Beijing Advanced Innovation Center for Genomics,  
6   Peking-Tsinghua Center for Life Sciences, Peking University Genome Editing Research Center,  
7   State Key Laboratory of Protein and Plant Gene Research, School of Life Sciences, Peking  
8   University, Beijing 100871, China. <sup>2</sup>Academy for Advanced Interdisciplinary Studies, Peking  
9   University, Beijing 100871, China. <sup>3</sup>NHC Key Laboratory of Systems Biology of Pathogens and  
10   Christophe Mérieux Laboratory, Institute of Pathogen Biology, Chinese Academy of Medical  
11   Sciences and Peking Union Medical College, Beijing 100730, China; Key Laboratory of  
12   Respiratory Disease Pathogenomics, Chinese Academy of Medical Sciences and Peking Union  
13   Medical College, Beijing 100730, China. <sup>4</sup>Biomedical Pioneering Innovation Center, Beijing  
14   Advanced Innovation Center for Genomics, Peking-Tsinghua Center for Life Sciences, Peking  
15   University, Beijing 100871, China.

16  
17   \*These authors contributed equally to this work.

18   †Email: [wswwei@pku.edu.cn](mailto:wswwei@pku.edu.cn) (W.W.)

19  
20   **Abstract:** SARS-CoV-2 has caused a worldwide pandemic. The emerging variants B.1.1.7 in the  
21   UK, B.1.351 in South Africa, and P.1 in Brazil have recently spread rapidly, arousing concerns  
22   about the efficacy of the current vaccines and antibody therapies. Therefore, there is still a high  
23   demand for alternative vaccines with great efficacy, high design flexibility, and fast manufacturing  
24   speed. Here, we reported a circular RNA (circRNA) vaccine that encodes the trimeric RBD of  
25   SARS-CoV-2 spike protein. Being a circularized RNA molecule, circRNA<sup>RBD</sup> could be rapidly  
26   produced via *in vitro* transcription and is highly stable without nucleotide modification. Lipid-  
27   nanoparticle-encapsulated circRNA<sup>RBD</sup> elicited potent and sustained neutralizing antibodies, as  
28   well as Th1-biased T cell responses in mice. Notably, antibodies from mice immunized with  
29   circRNA encoding RBD variant (K417N-E484K-501Y) effectively neutralized B.1.351 variant.

30 Moreover, we developed therapeutic circRNAs, encoding SARS-CoV-2 neutralizing nanobodies  
31 or hACE2 decoys, which could effectively neutralize SARS-CoV-2 pseudovirus. Our study  
32 suggests that circular RNA holds the potential to become a novel vaccine and therapeutic platform.

33

#### 34 **Main Text:**

35 Coronavirus disease 2019 (COVID-19) is a serious worldwide public health emergency caused by  
36 a novel severe acute respiratory syndrome coronavirus (SARS-CoV-2) (1, 2). To date, COVID-19  
37 has resulted in more than one hundred million confirmed cases and over two million confirmed  
38 deaths (World Health Organization). Thus, there is an urgent need for the development of safe and  
39 effective vaccines against SARS-CoV-2 infection.

40 SARS-CoV-2, together with Severe Acute Respiratory Syndrome (SARS)-CoV and Middle  
41 East Respiratory Syndrome (MERS)-CoV, other two highly pathogenic coronaviruses, belongs to  
42 the genus *Betacoronavirus* of the *Coronaviridae* family (3). SARS-CoV-2 is a single-strand,  
43 positive-sense, enveloped virus, and its virion is composed of an inner capsid formed by 30-kb  
44 RNA genome wrapped by the nucleocapsid (N) proteins and a lipid envelope coated with the  
45 membrane (M), envelope (E), and trimeric spike (S) proteins (4). The S protein of SARS-CoV-2,  
46 composed of S1 and S2 subunits, is the major surface protein of the virion. The S protein mediates  
47 viral entry into host cells by binding to its receptor, angiotensin-converting enzyme 2 (ACE2),  
48 through the receptor-binding domain (RBD) at the C terminus of the S1 subunit. This binding  
49 subsequently induces the fusion between the SARS-CoV-2 envelope and the host cell membrane  
50 mediated by the S2 subunit, leading to the release of the viral genome into the cytoplasm (5-8).

51 The S protein, S1 subunit, or the RBD antigen of SARS-CoV-2, could induce both B cell and T  
52 cell responses, generating highly potent neutralizing antibodies against SARS-CoV-2 (9-11).  
53 Vaccination is the most promising approach to end COVID-19 pandemic. Traditional vaccine  
54 platforms, such as inactivated vaccines, virus-like particle vaccines, and viral vector-based  
55 vaccines have been adopted to develop SARS-CoV-2 vaccines (12-20). Importantly, the mRNA  
56 vaccines against SARS-CoV-2 have been developed at warp speed and urgently approved for use  
57 (21-27), despite the fact that such strategy had never been applied commercially before (28). The  
58 mRNA vaccine contains a linear single-strand RNA, consisting of 5' cap, the untranslated region  
59 (UTR), antigen-coding region, and 3' polyA tail, which is delivered into bodies via lipid-nano

60 particle (LNP) encapsulation (28). The clinical-scale mRNA vaccines could be manufactured  
61 rapidly upon the viral antigen sequence is released (21). However, the current mRNA vaccine still  
62 has certain limitations due to its inherent instability and suboptimal thermostability after LNP  
63 encapsulation for *in vivo* administration (29-31), as well as potential immunogenic side effects (32,  
64 33).

65 Circular RNAs (circRNAs) are covalently closed single-stranded RNA transcripts, comprising  
66 a large class of non-coding RNAs generated by a non-canonical RNA splicing event called  
67 backsplicing in eukaryotic cells (34-36). Some viral genomes happen to be circular RNAs, such as  
68 hepatitis D virus and plant viroids (33). In recent years, thousands of circRNAs have been  
69 identified in eukaryotes, including fungi, plants, insects, fish, and mammals via high-throughput  
70 RNA sequencing and circRNA-specific bioinformatics (36). Unlike linear mRNA, circRNA is  
71 highly stable as its covalently closed ring structure protects it from exonuclease-mediated  
72 degradation (36-38). So far, only a few endogenous circRNAs have been shown to function as  
73 protein translation templates (39-42). Although circRNA lacks the essential elements for cap-  
74 dependent translation, it can be engineered to enable protein translation through internal ribosome  
75 entry site (IRES) or the m6A modification incorporated to its 5' UTR region (43, 44).

76 Here, we developed circRNA vaccines against the native SARS-CoV-2 or its emerging  
77 variants, which induced robust neutralizing antibodies and strong T cell responses in mice.  
78 Moreover, circRNA could be employed to express nanobodies or AEC2 decoys to neutralize the  
79 SARS-CoV-2 pseudovirus, manifesting its therapeutics potential to directly blockade such deadly  
80 infections.

81

## 82 ***In Vitro* circRNA production by Group I ribozyme autocatalysis**

83 We adopted a Group I ribozyme autocatalysis strategy (43) to produce circular RNA encoding  
84 SARS-CoV-2 RBD antigens (23), termed circRNA<sup>RBD</sup> (Fig. 1A). To enhance the immunogenicity  
85 of RBD antigens, we added a signal peptide sequence (SP) to the N-terminus of RBD for its  
86 secretory expression (45-47). In this construct, the IRES element was placed before the RBD-  
87 coding sequence to initiate its translation. The signal peptide sequence of human tissue  
88 plasminogen activator (tPA) (17, 45) was fused to the N-terminus of RBD to ensure the secretion  
89 of antigens, and the trimerization motif of bacteriophage T4 fibritin protein (foldon) (48) was fused

90 to its C terminus, mimicking the natural conformation of SARS-CoV-2 Spike trimers, which have  
91 a superior hACE2 binding capacity to the monomeric RBD counterparts (6, 7, 49). This IRES-SP-  
92 RBD-T4 sequence was then inserted into the cyclization vector (Fig. 1A) to generate the template  
93 for *in vitro* transcription (IVT) in order to produce circRNA<sup>RBD</sup>. The circularization of circRNA<sup>RBD</sup>  
94 was verified (Fig. 1B) by reverse transcription and RT-PCR analysis using specific primers (Fig.  
95 1A).

96 Owing to this covalently closed circular structure, the circRNA<sup>RBD</sup> migrated faster in  
97 electrophoresis (fig. S1A) and appeared more resistant to exonuclease RNase R than the linear  
98 RNAs (fig. S1B). Moreover, the high-performance liquid chromatography (HPLC) purification  
99 showed that the RNase R treatment purged significant amount of the linear precursor RNAs, an  
100 important step for the production and purification of the circRNA<sup>RBD</sup> (fig. S1C).

101

## 102 **Thermal stable circRNA<sup>RBD</sup> produces functional SARS-CoV-2 RBD antigens**

103 To test the secretory expression of RBD produced by circRNA<sup>RBD</sup>, the purified circRNA<sup>RBD</sup> was  
104 transfected into HEK293T cells. We detected ample production of SARS-CoV-2 RBD antigens in  
105 the supernatant by Western blot (Fig. 1C). Quantitative ELISA assay showed that the RBD protein  
106 reached ~143 ng/mL in the supernatant, 50-fold more than the linear RNA<sup>RBD</sup> group (Fig. 1D). We  
107 further confirmed that circRNA<sup>RBD</sup> could be expressed in murine NIH3T3 cells (Fig. 1E). Together,  
108 these results demonstrated that robust secretory RBD antigens could be produced using  
109 circRNA<sup>RBD</sup> in both human and murine cells.

110 The inherent stability of circRNA has been reported (50), and such a feature would make  
111 circRNA an attractive vaccine candidate. To test this, circRNA<sup>RBD</sup> was stored at room temperature  
112 (~25°C) for various days before transfected into HEK293T cells. We found that circRNA<sup>RBD</sup> could  
113 be readily expressed without detectable loss even after two weeks of shelf time (Fig. 1F),  
114 highlighting its remarkable thermal stability.

115 To further verify whether the secreted SARS-CoV-2 RBD antigens produced by circRNA<sup>RBD</sup>  
116 were functional, the supernatants of circRNA<sup>RBD</sup>-transfected cells were used for competition assay  
117 using hACE2-overexpressing HEK293 cells (HEK293T-ACE2) and SARS-CoV-2 pseudovirus  
118 harboring an EGFP reporter (51). We witnessed that the secreted SARS-CoV-2 RBD antigens

119 could effectively block SARS-CoV-2 pseudovirus infection (Fig. 1G and fig. S2). Altogether,  
120 circRNA<sup>RBD</sup> showed robust protein expression and high thermal stability, illuminating its potential  
121 for vaccination.

122

### 123 **SARS-CoV-2 circRNA vaccines elicit sustained humoral immune responses with high-level** 124 **neutralizing antibodies**

125 With its stability and immunogen-coding capability, we reasoned that circRNA could be developed  
126 into a new type of vaccine. We then attempted to assess the immunogenicity of circRNA<sup>RBD</sup>  
127 encapsulated with lipid nanoparticle in BALB/c mice (Fig. 2A). The circRNA<sup>RBD</sup> encapsulation  
128 efficiency was greater than 93%, with an average size of 100 nm in diameter (Fig. 2B). Animals  
129 were immunized with LNP-circRNA<sup>RBD</sup> through intramuscular injection twice, using a dose of 10  
130  $\mu\text{g}$  or 50  $\mu\text{g}$  per mouse at a two-week interval, while empty LNP was used as the placebo (Fig.  
131 2C). The amount of RBD-specific IgG and pseudovirus neutralization activity were evaluated at  
132 two or five weeks post LNP-circRNA<sup>RBD</sup> boost.

133 High titers of RBD-specific IgG were elicited by circRNA<sup>RBD</sup> in a dose-dependent manner,  
134  $\sim 3 \times 10^4$  and  $\sim 1 \times 10^6$  for each dose and for both 2- and 5-weeks post boost, indicating that  
135 circRNA<sup>RBD</sup> could induce long-lasting antibodies against SARS-CoV-2 RBD (Fig. 2D).

136 To test the antigen-specific binding capability of IgG from vaccinated animals, we performed a  
137 surrogate neutralization assay (52). In line with the amount of RBD-specific IgG (Fig. 2D),  
138 antibodies elicited by circRNA<sup>RBD</sup> vaccines showed evident neutralizing capacity in dose-  
139 dependent manner, with an NT50 of  $\sim 2 \times 10^4$  for the dose of 50  $\mu\text{g}$  (Fig. 2, E and F).

140 We further demonstrated that sera from circRNA<sup>RBD</sup>-vaccinated mice neutralized SARS-CoV-  
141 2 pseudovirus (Fig. 2G), with an NT50 of  $\sim 5.6 \times 10^3$  in mice immunized with 50  $\mu\text{g}$  of circRNA<sup>RBD</sup>  
142 vaccine. The large amount of RBD-specific IgG, potent RBD antigen neutralization, and sustained  
143 SARS-CoV-2 pseudovirus neutralizing capacity suggest that circRNA<sup>RBD</sup> vaccines did induce a  
144 long-lasting humoral immune response in mice.

145

### 146 **SARS-CoV-2 circRNA vaccines induce strong T cell immune responses in the spleen**

147 B cells (the source of antibodies), CD4<sup>+</sup> T cells, and CD8<sup>+</sup> T cells are three pillars of adaptive

148 immunity, and they mediated effector functions that have been associated with the control of  
149 SARS-CoV-2 in both non-hospitalized and hospitalized cases of COVID-19 (53).

150 To probe CD4<sup>+</sup> and CD8<sup>+</sup> T cell immune responses in circRNA<sup>RBD</sup> vaccinated mice (5 weeks  
151 post-boost), splenocytes were stimulated with SARS-CoV-2 Spike RBD pooled peptides (Table  
152 S1), and cytokine-producing T cells were quantified by intracellular cytokine staining among  
153 effector memory T cells (Tem, CD44<sup>+</sup>CD62L<sup>-</sup>) (fig. S3). Stimulated with RBD peptide pools,  
154 CD4<sup>+</sup> T cells of mice immunized with circRNA<sup>RBD</sup> vaccines exhibited Th1-biased responses,  
155 producing interferon- $\gamma$  (IFN- $\gamma$ ), tumor necrosis factor (TNF- $\alpha$ ), and interleukin-2 (IL-2) (Fig. 3, A  
156 and B), but not interleukin-4 (IL-4) (fig. S4), indicating that circRNA<sup>RBD</sup> vaccines mainly induced  
157 the Th1- but not the Th2-biased immune responses. In addition, multiple cytokine-producing CD8<sup>+</sup>  
158 were detected in circRNA<sup>RBD</sup> vaccinated mice (Fig. 3, C and D). For unknown reasons, 10  $\mu$ g of  
159 circRNA<sup>RBD</sup> elicited stronger immune responses in both CD4<sup>+</sup> and CD8<sup>+</sup> effector memory T cells  
160 than 50  $\mu$ g (Fig. 3, A to D), while the latter induced higher potency of neutralizing antibodies in  
161 the B cell responses (Fig. 2G).

162 Collectively, these results demonstrated that SARS-CoV-2 circRNA<sup>RBD</sup> vaccines could induce  
163 high level of humoral and cellular immune responses in mice.

164

### 165 SARS-CoV-2 circRNA<sup>RBD-501Y.V2</sup> vaccines show preferential neutralization activity against 166 B.1.351 variant

167 Next, we evaluated the efficacy of a circRNA vaccine encoding RBD/K417N-E484K-N501Y  
168 derived from the B.1.351/501Y.V2 variant, termed as circRNA<sup>RBD-501Y.V2</sup> (Fig. 4A). BALB/c mice  
169 were immunized with an i.m. injection of the circRNA<sup>RBD-501Y.V2</sup> vaccine, followed by a boost at a  
170 two-week interval. The immunized mice's sera were collected at 1 and 2 weeks post the boost. The  
171 ELISA showed that the RBD-501Y.V2-specific IgG titer reached  $7 \times 10^4$  at 2 weeks post boost (Fig.  
172 4B). The surrogate neutralization assay showed that sera of circRNA<sup>RBD-501Y.V2</sup> immunized mice  
173 effectively neutralized RBD antigens (Fig. 4C). We then went on to assess the neutralization  
174 activity of the sera from mice immunized with circRNA<sup>RBD</sup> or circRNA<sup>RBD-501Y.V2</sup> vaccines against  
175 D614G, B.1.1.7/501Y.V1, or B.1.351/501Y.V2 variants. VSV-based pseudovirus neutralization  
176 assay revealed that antibodies elicited by circRNA<sup>RBD</sup> vaccines, which encode the native RBD  
177 sequence, effectively neutralized all three viral strains, with the highest activity against the D614G



178 strain (Fig. 4D). The circRNA<sup>RBD-501Y.V2</sup> immunized mouse serum could also neutralize all three  
179 pseudoviruses, with the highest neutralization activity against its corresponding variant, 501Y.V2  
180 (Fig. 4E). Collectively, circRNA vaccines-elicited antibodies showed the best neutralization  
181 activity against their corresponding variant strains. It's worth noting that both vaccines could  
182 neutralize all three strains albeit with variable efficacies. Nevertheless, the multivalent vaccines  
183 should have provided better protection for both native SARS-CoV-2 strain and its circulating  
184 variants.

185

### 186 **Expression of SARS-CoV-2 neutralizing antibodies via circRNA platform**

187 Besides vaccine, circRNA could be re-purposed for therapeutics when used to express some other  
188 proteins or peptides, such as enzymes for rare diseases and antibodies for infectious diseases or  
189 cancer. Here, we attempted to test the therapeutic potential of circRNAs by expressing the SARS-  
190 CoV-2 neutralizing antibodies. It has been reported that SARS-CoV-2 neutralizing nanobodies or  
191 hACE2 decoys could inhibit the SARS-CoV-2 infection (54-56). This prompted us to leverage the  
192 circRNA platform to express SARS-CoV-2 neutralizing nanobodies, including nAB1, nAB1-Tri,  
193 nAB2, nAB2-Tri, nAB3, and nAB3-Tri (54, 55), together with hACE2 decoys (56) (Fig. 5A).  
194 Pseudovirus neutralizing assay showed that supernatants of HEK293T cells transfected with  
195 circRNA<sup>nAB</sup> or circRNA<sup>hACE2 decoys</sup> could effectively inhibit pseudovirus infection (Fig. 5B).  
196 Among those, nAB1-Tri, nAB2, nAB2-Tri, and nAB3-Tri nanobodies produced by circRNAs  
197 completely blocked pseudovirus infection.

198

### 199 **Discussion**

200 COVID-19 is still a fast-growing global health crisis with circulating SAS-CoV-2 variants evading  
201 current vaccines elicited antibodies (57-59). This report established a novel approach using  
202 circRNA to produce SARS-CoV-2 related interventions, including vaccine, therapeutic  
203 nanobodies, and hACE2 decoys.

204 Several studies have reported that the full-length Spike protein (mRNA-1273 and BNT162b2)  
205 (21, 22, 27) or RBD-based mRNA vaccines elicit neutralizing antibodies and cellular immune  
206 responses (23-26, 60). As reported, most effective neutralizing antibodies recognize the RBD

207 region of S protein (54, 55, 61-64) and targeting RBD may induce less amount of non-neutralizing  
208 antibodies (23-26, 60). Given that RBD trimers were superior in binding hACE2 compared to their  
209 monomeric counterparts (49), we chose to express RBD trimers as the immunogen.

210 We highlight this generalizable strategy for designing immunogens. The coding sequence of  
211 circular RNA can be quickly adapted to deal with any emerging SARS-CoV-2 variants, such as  
212 the recently reported B.1.1.7/501Y.V1, B.1.351/501Y.V2, and P.1 variants (58, 65, 66). Moreover,  
213 circular RNAs could be quickly generated in large quantities *in vitro*, and they do not require any  
214 nucleotide modification, strikingly different from the canonical mRNA vaccines. Interestingly,  
215 circular RNA itself could serve as a vaccine adjuvant (33), suggesting that circRNA vaccine is  
216 likely benefit from its own adjuvant effect.

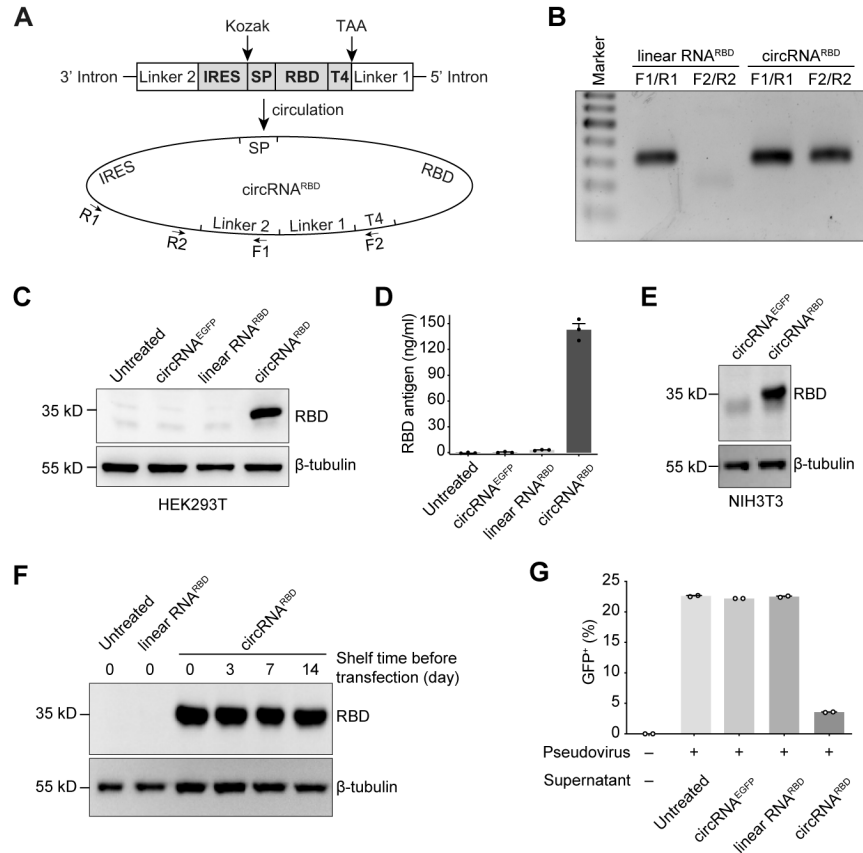
217 In this report, circRNA<sup>RBD-501Y.V2</sup> immunized mice produced high titers of neutralizing  
218 antibodies. Given that K417N-E484K-N501Y mutant in RBD reduces its interactions with certain  
219 neutralizing antibodies (58, 67), we also demonstrated that neutralizing antibodies produced by  
220 mice immunized with circRNA<sup>RBD</sup> or circRNA<sup>RBD-501Y.V2</sup> had preferential neutralizing abilities to  
221 their corresponding virus strains.

222 Multiple candidates for the treatment of COVID-19 have been studied during the pandemic,  
223 especially those neutralizing antibodies (54, 55, 61-64) and engineered soluble natural receptor for  
224 the virus, hACE2 (68, 69). circRNA-encoded SARS-CoV-2 neutralizing nanobodies or hACE2  
225 decoy all showed strong neutralizing ability *in vitro*. Given that SARS-CoV-2 variants encoding  
226 E484K or N501Y or the K417N-E484K-N501Y evade certain neutralizing antibodies induced by  
227 mRNA vaccines (58, 67), we anticipated that the effect of circRNA-encoded hACE2 decoy might  
228 not be affected by virus mutations.

229 Owing to their specific properties, circRNAs hold potentials in biomedical applications.  
230 Nevertheless, the immunogenicity and the safety of circular RNA vaccines or drugs await further  
231 investigations.

232





233

234 **Fig. 1. Expression of trimeric SARS-CoV-2 RBD antigens with circular RNAs *in vitro*.** (A)

235 Schematic diagram of circRNA<sup>RBD</sup> circularization by the Group I ribozyme autocatalysis. SP,

236 signal peptide sequence of human tPA protein. T4, the trimerization domain from bacteriophage

237 T4 fibrin protein. RBD, the receptor binding domain of SARS-CoV-2 Spike protein. The arrows

238 indicate the the design of primers for PCR analysis. (B) The agarose gel electrophoresis result of

239 the PCR products of linear RNA<sup>RBD</sup> and circRNA<sup>RBD</sup>. (C) Western Blot analysis showing the

240 expression level of RBD antigens in the supernatant of HEK293T cells transfected with

241 circRNA<sup>RBD</sup>. The circRNA<sup>EGFP</sup> and linear RNA<sup>RBD</sup> were set as controls. (D) The quantitative

242 ELISA assay to measure the concentration of RBD antigens in the supernatant. The data in (B)

243 was shown as the mean ± S.E.M. (n = 3). (E) Western Blot analysis showing the expression level

244 of RBD antigens in the supernatant of mouse NIH3T3 cells transfected with circRNA<sup>RBD</sup>. The

245 circRNA<sup>EGFP</sup> was set as controls. (F) Western Blot analysis showing the expression level of RBD

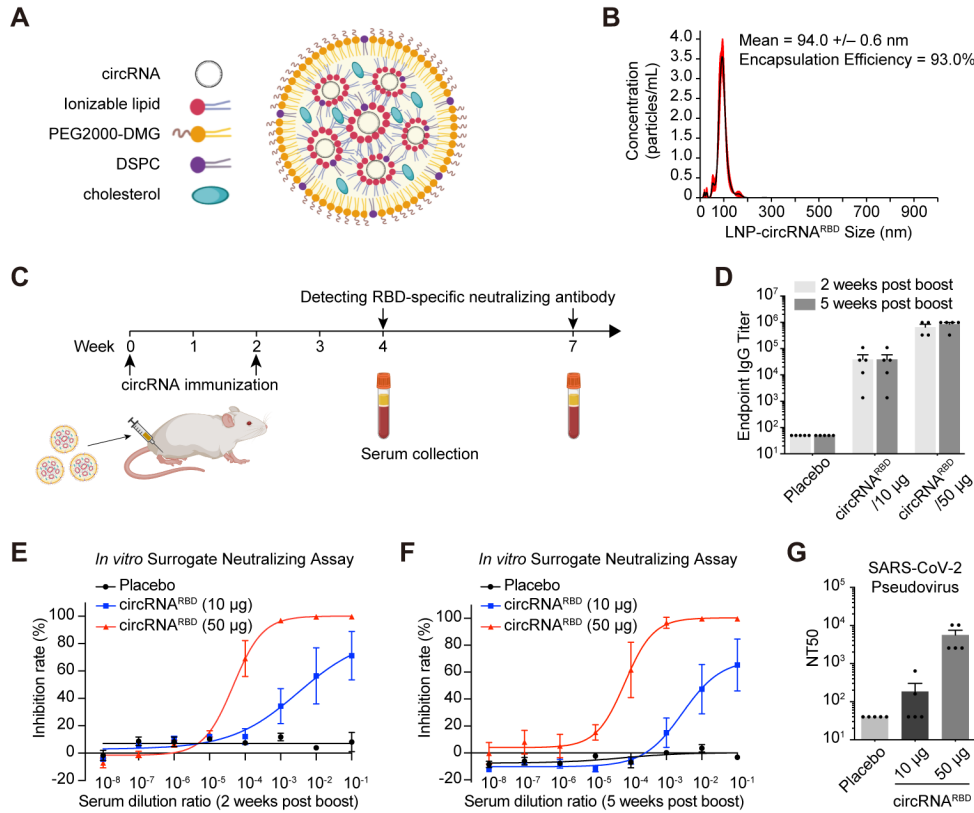
246 antigens in the supernatant of HEK293T cells transfected with circRNA<sup>RBD</sup> for different shelf time

247 (3, 7 or 14 days) at room temperature (~25°C). (G) Quantification of the competitive inhibition of

248 SARS-CoV-2 pseudovirus infection (EGFP) by the circRNA<sup>RBD</sup>-translated RBD antigens. The

249 circRNA<sup>EGFP</sup> and linear RNA<sup>RBD</sup> were set as controls. The data in (E) was shown as the mean ±  
250 S.E.M. (n = 2).

251



252

253 **Fig. 2. Humoral immune responses in mice immunized with SARS-CoV-2 circRNA<sup>RBD</sup>**

254 **vaccines. (A)** Schematic representation of LNP-circRNA complex. **(B)** Representative of

255 concentration-size graph of LNP-circRNA<sup>RBD</sup> measured by dynamic light scattering method. **(C)**

256 Schematic diagram of the LNP-circRNA<sup>RBD</sup> vaccination process in BALB/c mice and serum

257 collection schedule for specific antibodies analysis. **(D)** Measuring the SARS-CoV-2 specific IgG

258 antibody titer with ELISA. The data were shown as the mean ± S.E.M. (n = 4 or 5). **(E)** Sigmoidal

259 curve diagram of the inhibition rate by sera of immunized mice with surrogate virus neutralization

260 assay. Sera from circRNA<sup>RBD</sup> (10 μg) and circRNA<sup>RBD</sup> (50 μg) immunized mice were collected at

261 2 weeks post the second dose. The data was shown as the mean ± S.E.M. (n = 4). **(F)** Sigmoidal

262 curve diagram of the inhibition rate by sera of immunized mice with surrogate virus neutralization

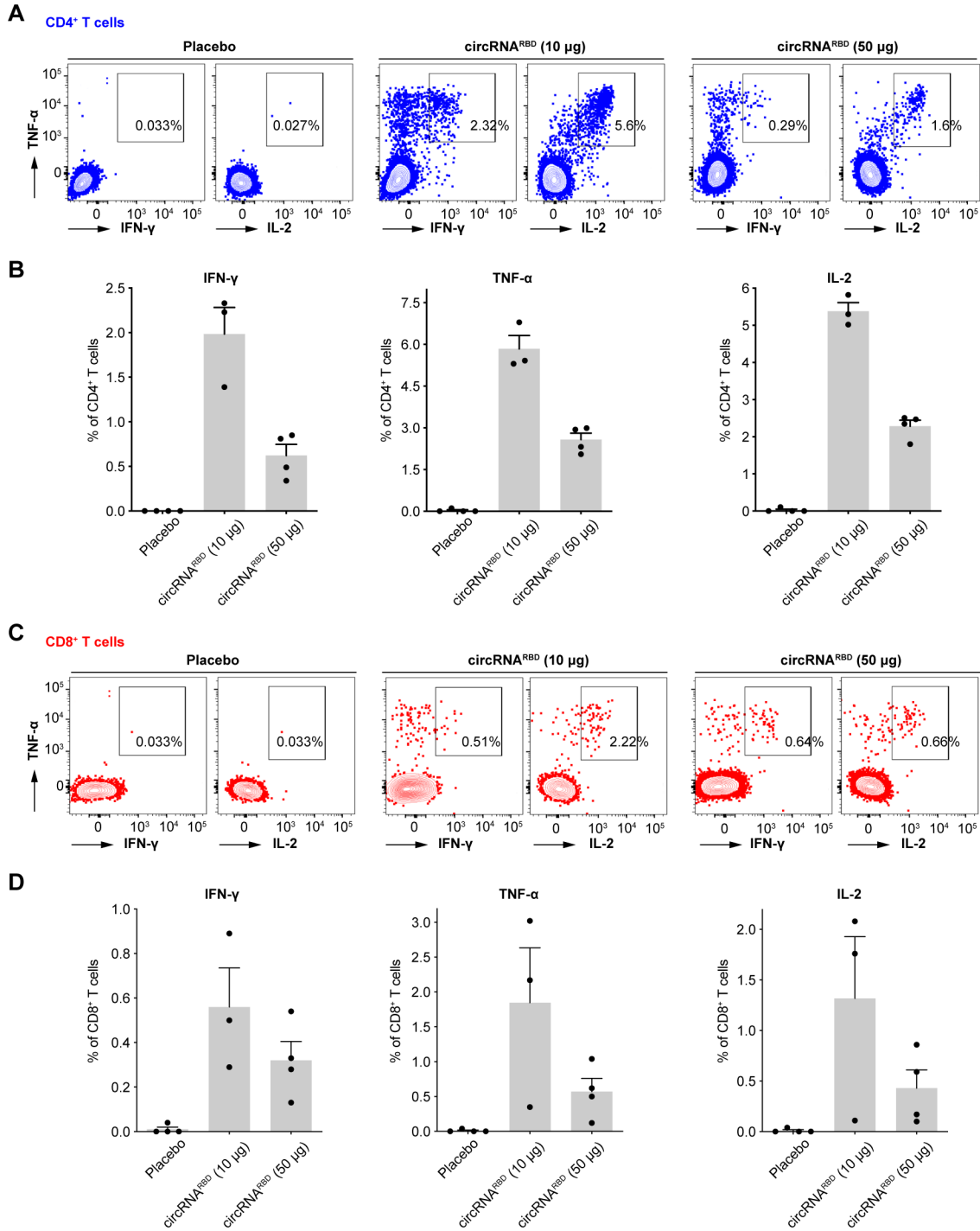
263 assay. Sera from circRNA<sup>RBD</sup> (10 μg) and circRNA<sup>RBD</sup> (50 μg) immunized mice were collected at

264 5 weeks post boost. The data were shown as the mean ± S.E.M. (n = 5). **(G)** The NT50 was

265 calculated using lentivirus-based SARS-CoV-2 pseudovirus. The data was shown as the mean ±

266 S.E.M. (n = 5).

267

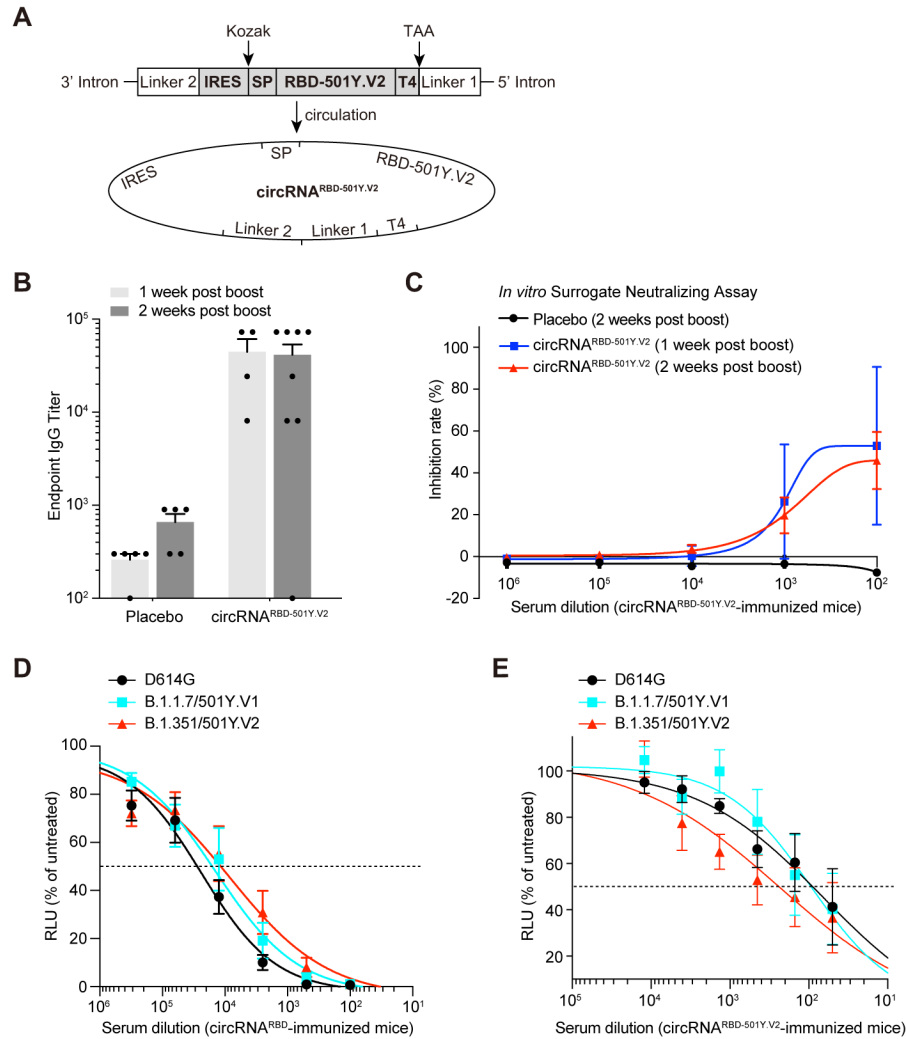


268

269 **Fig. 3. SARS-CoV-2 specific T cell immune responses in mice immunized with SARS-CoV-2**  
 270 **circRNA<sup>RBD</sup> vaccines.** (A) The FACS analysis results showing the percentages of cytokine  
 271 positive cells evaluated among single and viable CD4<sup>+</sup>CD62L<sup>-</sup>CD4<sup>+</sup> T cells. (B) The intracellular  
 272 staining assay for cytokines (IFN-γ, TNF-α, and IL-2) production among SARS-CoV-2 specific  
 273 CD4<sup>+</sup> effector memory T cells (CD4<sup>+</sup>CD62L<sup>-</sup>) in splenocytes. (C) The FACS analysis results

274 showing the percentages of cytokine positive cells evaluated among single and viable  
275 CD44<sup>+</sup>CD62L<sup>-</sup>CD8<sup>+</sup> T. **(D)** The intracellular staining assay for cytokines (IFN- $\gamma$ , TNF- $\alpha$ , and IL-  
276 2) production among SARS-CoV-2 specific CD8<sup>+</sup> effector memory T cells (CD44<sup>+</sup>CD62L<sup>-</sup>) in  
277 splenocytes. Results were pooled from two independent experiments (**B** and **D**). Data are presented  
278 as the mean  $\pm$  S.E.M. in C and D, n = 3 or 4 for each group. Each symbol represents an individual  
279 mouse.

280



281

282 **Fig. 4. The susceptibility of SARS-CoV-2 D614G, B.1.1.7 or B.1.351 variants to neutralizing**

283 **antibodies elicited by the circRNA<sup>RBD</sup> or circRNA<sup>RBD-501Y.V2</sup> vaccines in mice. (A) Schematic**

284 **diagram of circRNA<sup>RBD-501Y.V2</sup> circularization by the Group I ribozyme autocatalysis. SP, signal**

285 **peptide sequence of human tPA protein. T4, the trimerization domain from bacteriophage T4**

286 **fibrin protein. RBD-501Y.V2, the RBD antigen harboring the K417N-E484K-N501Y mutations**

287 **in SARS-CoV-2 501Y.V2 variant. (B) Measuring the SARS-CoV-2 specific IgG antibody titer with**

288 **ELISA. The data was shown as the mean  $\pm$  S.E.M. Each symbol represents an individual mouse.**

289 **(C) Sigmodal curve diagram of the inhibition rate by sera of immunized mice with surrogate virus**

290 **neutralization assay. Sera from circRNA<sup>RBD-501Y.V2</sup> (50  $\mu$ g) immunized mice were collected at 1**

291 **week or 2 weeks post boost. The data were shown as the mean  $\pm$  S.E.M. (D) Neutralization assay**

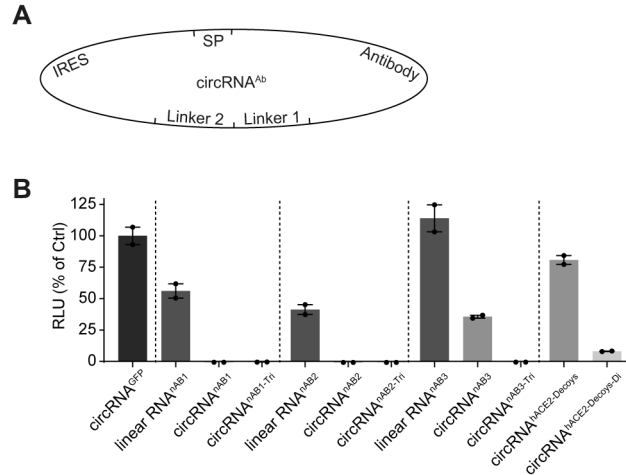
292 **of VSV-based D614G, B.1.1.7 or B.1.351 pseudovirus with the serum of mice immunized with**

293 **circRNA<sup>RBD</sup> vaccines. The serum samples were collected at 5 weeks post boost. The data were**

294 shown as the mean  $\pm$  S.E.M. (n = 5). (E) Neutralization assay of VSV-based D614G, B.1.1.7 or  
295 B.1.351 pseudovirus with the serum of mice immunized with circRNA<sup>RBD-501Y.V2</sup> vaccines. The  
296 serum samples were collected at 1 week post boost. The data were shown as the mean  $\pm$  S.E.M. (n  
297 = 5).

298





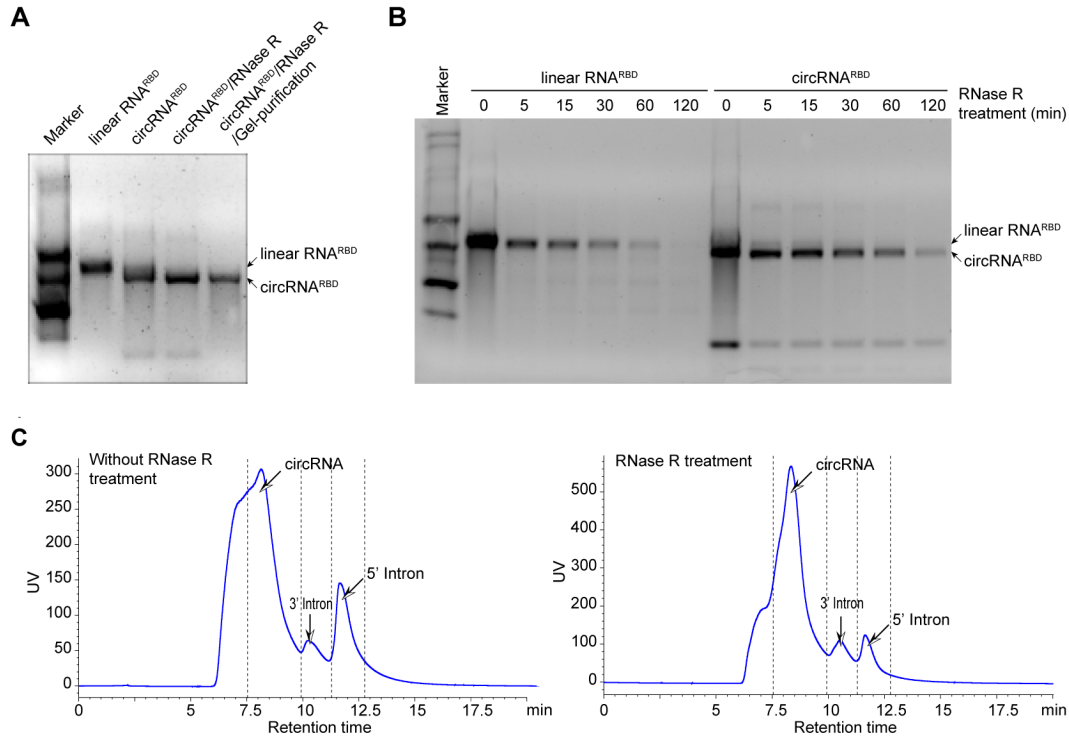
299

300 **Fig. 5. Expression of SARS-CoV-2 neutralizing nanobodies or hACE2 decoys via circRNA**  
301 **platform.** (A) Schematic diagram of circRNA<sup>nAB</sup> or circRNA<sup>hACE2 decoys</sup> circularization by the  
302 Group I ribozyme autocatalysis. (B) Lentiviral-based pseudovirus neutralization assay with the  
303 supernatant from cells transfected with circRNA encoding neutralizing nanobodies nAB1, nAB1-  
304 Tri, nAB2, nAB2-Tri, nAB3 and nAB3-Tri or ACE2 decoys. The luciferase value was normalized  
305 to the circRNA<sup>EGFP</sup> control. The data was shown as the mean  $\pm$  S.E.M. (n = 2).

306

307

308 **Supplementary Figure Legends**

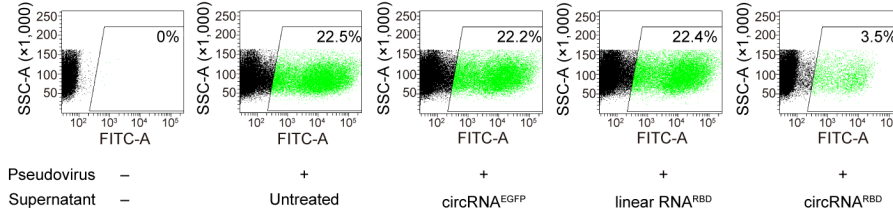


309

310 **fig S1: Agarose gel electrophoresis and HPLC purification of circRNA<sup>RBD</sup>.** (A) The agarose  
311 gel electrophoresis result of linear RNA<sup>RBD</sup> and circRNA<sup>RBD</sup> with different treatment. (B) The  
312 agarose gel electrophoresis result of circRNA<sup>RBD</sup> and linear RNA<sup>RBD</sup> digested by RNase R with  
313 various time from 5 min to 120 min. (C) HPLC chromatogram of circRNA<sup>RBD</sup> without RNase R  
314 treatment (left) and circRNA<sup>RBD</sup> treated by RNase R (right).

315

316

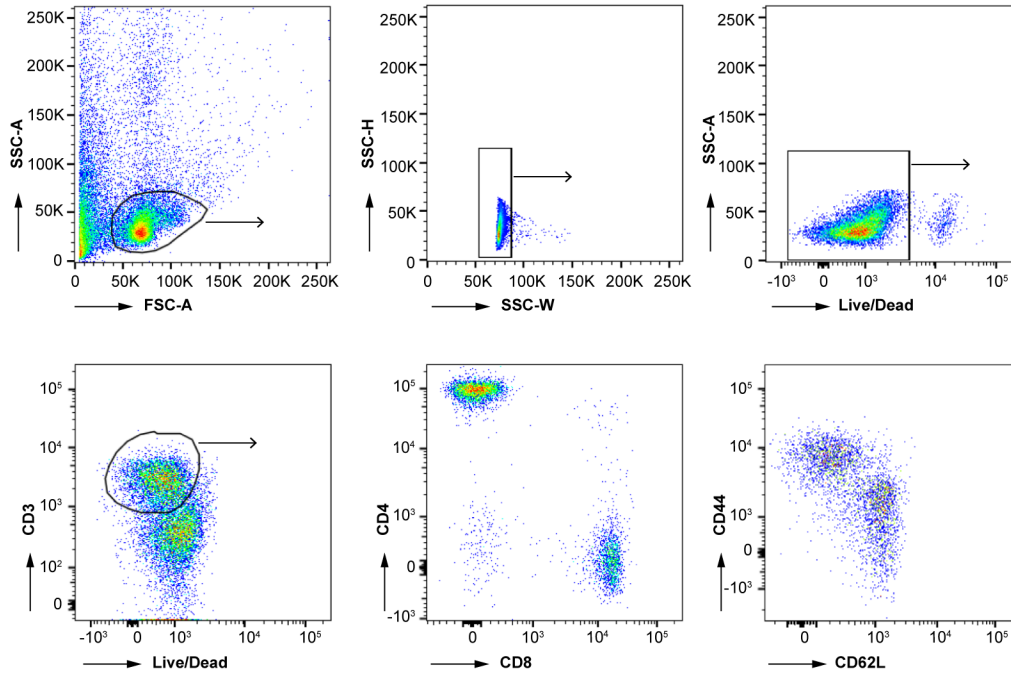


317

318 **fig S2: The FACS chromatogram of the competitive inhibition of SARS-CoV-2 pseudovirus**  
319 **infection (harboring EGFP reporter) by the circRNA<sup>RBD</sup>-translated RBD antigens.**

320

321

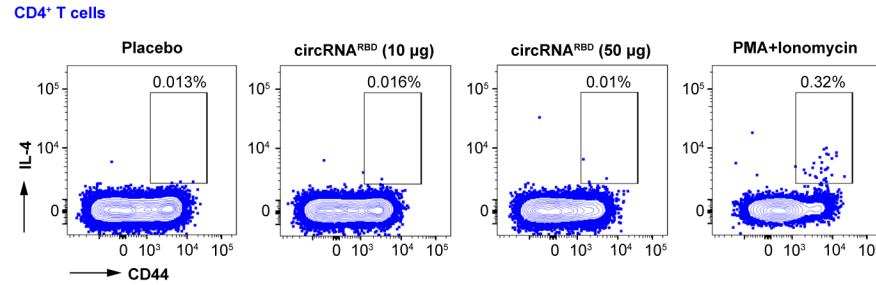


322

323 **fig S3: Flow panel and gating strategy to quantify SARS-CoV-2-RBD-specific T cells in**  
324 **mice.** The plots showed the gating strategy of single and viable T cells from spleens. CD4<sup>+</sup> or  
325 CD8<sup>+</sup> T cells were further analyzed with the expression of CD44 and CD62L.

326

327



328

329 **fig S4: Identification of IL-4 producing CD4<sup>+</sup> T cells in mice immunized with SARS-CoV-2**  
330 **circRNA<sup>RBD</sup> vaccines.** Splenocytes were stimulated with SARS-CoV-2-RBD peptides for 7 hr in  
331 the presence of BFA and Monensin. PMA and Ionomycin stimulation were applied as a positive  
332 control. Cells were gated on single and viable CD4<sup>+</sup> T cells. The plots are representative for two  
333 independent experiments with same results.

334

335

## 336 **Materials and methods**

### 337 *Cell culture*

338 HEK293T and NIH3T3 cell lines were maintained in our laboratory. The HEK293T-hACE2 cell  
339 line was ordered from Biodragon Inc. (#BDAA0039, Beijing, China). These mammalian cell lines  
340 were cultured in Dulbecco's Modified Eagle Medium (Corning, 10-013-CV) with 10% fetal bovine  
341 serum (FBS) (BI), supplemented with 1% penicillin-streptomycin in 5% CO<sub>2</sub> incubator at 37°C.  
342 The Huh-7 cells were maintained in Xie laboratory at Peking University, cultured with the methods  
343 previously described (61).

344

### 345 *circRNA transfection in vitro*

346 For the circRNA transfection in HEK293T or NIH3T3 cells,  $3 \times 10^5$  cells per well were seeded in  
347 12-well plates. 4 µg of RNase R-treated or HPLC-purified & CIP-treated circRNAs were  
348 transfected into the HEK293T or NIH3T3 cells, 24 hr later, using Lipofectamine MessengerMax  
349 (Invitrogen, LMRNA003) according to the manufacturer's instructions. 48 hr post transfection,  
350 the cell lysis and supernatant were collected for the following detections.

351

### 352 *LNP encapsulation of circRNA*

353 The circRNAs were encapsulated with lipid nanoparticle (LNP) through a previously described  
354 process (70). Briefly, the circRNAs were diluted in the 50 mM citrate buffer (pH 3.0) and the lipids  
355 were dissolved and mixed in ethanol at molar ratios of 50:10:38.5:1.5 (MC3-  
356 lipid:DSPC:cholesterol:PEG2000-DMG). The lipids mixture was then mixed with the circRNA  
357 solution at the volume ratio of 1:3 in the NANOASSEMBLER BENCHTOP (PRECISION,  
358 #NIT0046). Then the LNP-circRNA formulations were diluted 40-fold with the 1×PBS buffer (pH  
359 7.2~7.4) and concentrated by ultrafiltration with Amicon® Ultra Centrifugal Filter Unit  
360 (Millipore). The concentration and encapsulation rate of circRNAs were measured by the Quant-  
361 iT™ RiboGreen™ RNA Assay Kit (Invitrogen™ #R11490). The size of LNP-circRNA particles  
362 was measured using dynamic light scattering on a Malvern Zetasizer Nano-ZS 300 (Malvern).  
363 Samples were irradiated with red laser ( $\lambda = 632.8$  nm) and scattered light were detected at a

364 backscattering angle of 173. Results were analyzed to obtain an autocorrelation function using the  
365 software (Zetasizer V7.13).

366

### 367 ***Circulation fragments PCR assay***

368 The circRNA<sup>RBD</sup> or linear RNA<sup>RBD</sup> was reverse transcribed into cDNA templates using specific  
369 primers with Quantscript RT Kit (KR103, TIANGEN). Then the internal control fragments and  
370 junction fragments were PCR amplified from the above cDNA templates with corresponding  
371 primers, respectively.

372

### 373 ***Quantitative determination of SARS-CoV-2 Spike RBD expression in vitro***

374 Quantification of RBD expression in cell culture supernatants was performed with a commercial  
375 SARS-CoV-2 Spike RBD Protein ELISA kit (RK04135, ABclonal) according to the  
376 manufacturer's instruction. The supernatants were diluted at 1:100 rate. Final concentrations of  
377 RBD were calculated basing on the linear standard curve of absorbance at 450 nm, using 630 nm  
378 as reference. Briefly, the detection wells were pre-coated with monoclonal antibody specific for  
379 Spike RBD protein. After incubation with samples or standards at 37°C for two hours, samples  
380 unbound to immobilized antibody would be removed by washing steps. Then the RBD-specific  
381 antibodies were added to wells for one-hour incubation at 37°C. After washing, the HRP substrates  
382 and stop solution were added and the absorbance at 450 nm were measured using 630 nm as  
383 reference.

384

### 385 ***Mouse vaccination and serum collection***

386 The BALB/c mice were ordered from Beijing Vital River Laboratory Animal Technology Co., Ltd.  
387 All mice were bred and kept under SPF (specific pathogen-free) conditions in the Laboratory  
388 Animal Center of Peking University. The animal experiments were approved by Peking University  
389 Laboratory Animal Center (Beijing), and undertaken in accordance with the National Institute of  
390 Health Guide for Care and Use of Laboratory Animals.



391 For mouse vaccination, groups of 6-8 week-old female BLAB/c mice were intramuscularly  
392 immunized with LNP-circRNA<sup>RBD</sup> (10 µg, N = 5; 50 µg, N = 5), or Placebo (empty LNP, N = 5)  
393 in 150 µL using a 1 mL sterile syringe, and 2 weeks later a second dose was immunized to boost  
394 the immune responses. The sera of immunized mice were collected at 2 and 5 weeks post the  
395 second immunization to detect the SARS-CoV-2-specific IgG titers and neutralizing antibody  
396 activity as described below. At 5 weeks post the second immunization, the immunized mice were  
397 sacrificed and the splenocytes were isolated for the detection of SARS-CoV-2-specific CD4<sup>+</sup> and  
398 CD8<sup>+</sup> T cell immune responses by Flow cytometry analysis and ELISA as described below.

399

#### 400 *Antibody titer measurement with ELISA*

401 All the immunized mouse serum samples were heat-inactivated at 56°C for 30 min before use. The  
402 SARS-CoV-2-specific IgG antibody titer was measured by ELISA. Briefly, serial 3-fold dilutions  
403 (in 1% BSA) of heat-inactivated sera, starting at 1:50, were added to the 96-well plates (100  
404 µL/well; Costar) coated with recombinant SARS-CoV-2 Spike antigens (Sino Biological) and  
405 blocked with 1% BSA, and the plates were incubated for at 37°C for 60 min. Then, after three  
406 washes with wash buffer, the Horseradish peroxidase HRP-conjugated rabbit anti-mouse IgG  
407 (Sigma) diluted in 1% BSA at 1:10,000 ratio (Sigma), was added to the plates and incubated at  
408 37°C for 45 min. Then the plates were washed for 4 times with wash buffer and added with TMB  
409 substrates (100 µL/well) followed by incubation for 15-20 min. And then the ELISA stop buffer  
410 was added into the plates. Finally, the absorbance (450/630 nm) was measured with Infinite M200  
411 (TECAN). The Endpoint IgG titers were defined as the dilution, which emitted an optical density  
412 exceeding 3x background (without serum but secondary antibody was added).

413

#### 414 *SARS-CoV-2 Surrogate Virus Neutralization Assay*

415 The neutralizing activity of mouse serum samples was detected by SARS-CoV-2 Surrogate Virus  
416 Neutralization Test Kit (L00847A, GenScript). Detections were performed according to  
417 manufacturer's instruction. Serial 10-fold dilutions of heat-inactivated sera, starting at 1:10, were  
418 incubated with HRP-conjugated RBD solutions at 37°C for half an hour, and then the mixtures  
419 were added into 96-well plates pre-coated with human ACE2 (hACE2) proteins and incubated for

420 15 min at 37°C. After washing the TMB substrates and stop solutions were added and the  
421 absorbance (450/630 nm) was measured with Infinite M200 (TECAN). The inhibition rates of  
422 serum samples were calculated according to the following formula. The half-neutralization titer of  
423 serum (NT50) was determined using four-parameter nonlinear regression in Prism 8 (GraphPad).

424 Inhibition rate = (1- OD value of sample/OD value of negative control) × 100%

425

#### 426 ***Pseudovirus-based neutralization assay***

427 The production of lentivirus-based SARS-CoV-2 pseudovirus and neutralization assay were  
428 performed as described previously (71). Briefly, the SARS-CoV-2 pseudovirus were produced by  
429 co-transfecting plasmids psPAX2 (6 µg), pSpike (6 µg), and pLenti-Luc-GFP (6 µg) into  
430 HEK293T cells using X tremeGENE HP DNA Transfection Reagent (Roche) according to the  
431 manufacturer's instructions. 48 hr post transfection, the supernatants containing pseudovirus  
432 particles were harvested and filtered through a 0.22-µm sterilized membrane for the neutralization  
433 assay as described below.

434 For the determination of NT50 of immunized mouse serum, the HEK293T-hACE2 cells were  
435 seeded in 96-well plates (50,000 cells/well) and incubated for approximate 24 hr until reaching  
436 over 90% confluent, preparing for pseudovirus infection. The mouse serum was 3-fold diluted,  
437 starting at 1:40, and incubated with the SARS-CoV-2 pseudovirus (MOI ≈ 0.05) at 37°C for 60  
438 min. The DMEM medium without serum was used as the negative control group. Then the  
439 supernatant of HEK293T-hACE2 cells were removed and the mixer of serum and pseudovirus  
440 were added to each well. 36-48 hr later, the luciferase activity, which reflecting the degree of  
441 SARS-CoV-2 pseudovirus transfection, was measured using the Nano-Glo Luciferase Assay  
442 System (Promega). The 50% neutralization titer (NT50) was defined as the fold-dilution, which  
443 emitted an exceeding 50% inhibition of pseudovirus infection in comparison with the control group.

444 The neutralization assay of VSV-based pseudovirus of SARS-CoV-2 and variants was performed  
445 as described previously (61, 62). Briefly, serum was diluted at 1:100 with 5 additional serial 5-  
446 fold dilution, and incubated with the same volume of pseudovirus with a TCID<sub>50</sub> of 1.3×10<sup>4</sup> for 60  
447 min at 37°C. 20,000 Huh-7 cells/well were cultured with mixture at 37°C for 24 h. Luciferase  
448 activity was measured using the britelite plus Reporter Gene Assay System (PerkinElmer).

449 Relative luciferase units (RLU) were normalized to untreated groups, and analyzed by four-  
450 parameter nonlinear regression in Prism (GraphPad).

451 For the neutralization assay of circRNA<sup>nAB</sup> or circRNA<sup>ACE2 decoys</sup>, the HEK293T-hACE2 cells  
452 were seeded in 96-well plates (50,000 cells/well) and incubated for approximate 24 hr until  
453 reaching over 90% confluent. The pseudovirus were pre-incubated with the supernatant of the  
454 circRNA<sup>nAB</sup> or circRNA<sup>ACE2 decoys</sup> transfected cells at 37°C for 60 min, and then added to cells in  
455 the 96-well plates. Media were changed at 24 hr after transduction. All cells were collected at 48  
456 hr after transduction. Luciferase activity was measured using the Nano-Glo Luciferase Assay  
457 System (Promega). The relative luminescence units were normalized to cells infected with  
458 supernatant of cell transfected with the circRNA<sup>EGFP</sup>.

459

#### 460 ***T cell flow cytometry analysis***

461 The Splenocytes from each immunized mouse were cultured in R10 media (RPMI 1640  
462 supplemented with 1% Pen-Strep antibiotic, 10% HI-FBS), stimulated with RBD peptide pools  
463 (Table S1) (Sangon Biotech) for 7 hr at 37°C with protein transport inhibitor cocktail (added 3 hr  
464 later). Peptide pools were used at a final concentration of 2 µg/mL for each peptide. Cells from  
465 each group were pooled for stimulation with cell stimulation cocktail (PMA/Ionomycin) as a  
466 positive control. Following stimulation, cells were washed with PBS prior to staining with  
467 LIVE/DEAD for 20 min at room temperature. Cells were then washed in stain buffer (PBS  
468 supplemented with 2.5% FBS) and suspended in Fc Block for 5 min at RT prior to staining with a  
469 surface stain of following antibodies: CD3 (Invitrogen, 45-0031-82)/CD4 (BD, 562285)/CD8 (BD,  
470 553035)/CD69 (BD, 557392)/CD44 (BD, 563058)/CD62L (BD, 560507). After 20 min, cells were  
471 washed with stain buffer, and then fixed and permeabilized using the BD Cytoperm  
472 fixation/permeabilization solution kit according to manufacturer instructions. Cells were washed  
473 in perm/wash solution, followed by intracellular staining (30 min, RT) using a cocktail of the  
474 following antibodies: IFN-γ (BD, 557998)/IL-2 (BD, 560547)/IL-4 (BD, 554435)/TNF-α (BD,  
475 557644). Finally, cells were washed in perm/wash solution and suspended in stain buffer. Samples  
476 were washed and acquired on a LSRFortessa (BD Biosciences). Analysis was performed using  
477 FlowJo software.

478

479 ***Expression of neutralizing nanobodies or ACE2 decoys by circular RNAs***

480 HEK293T cells were transfected with circular RNA in transfection reagent. Circular RNA  
481 encoding secretory nanobodies or hACE2 decoys were purified after GTP treatment for cyclization.  
482 In brief, HEK293T cells were seeded in 12-well plates. After 24 h, cells were transfected with  
483 circRNA (4 µg per well) and continuously added fresh medium to a final volume of about 1 ml.  
484 Supernatants were harvested at 48 hr post transfection and centrifuged to remove cells.

485

486 **REFERENCES**

- 487 1. F. Wu *et al.*, A new coronavirus associated with human respiratory disease in China. *Nature* **579**, 265-269  
488 (2020).
- 489 2. P. Zhou *et al.*, A pneumonia outbreak associated with a new coronavirus of probable bat origin. *Nature*  
490 **579**, 270-273 (2020).
- 491 3. P. V'Kovski, A. Kratzel, S. Steiner, H. Stalder, V. Thiel, Coronavirus biology and replication: implications  
492 for SARS-CoV-2. *Nat Rev Microbiol* **19**, 155-170 (2021).
- 493 4. D. Kim *et al.*, The Architecture of SARS-CoV-2 Transcriptome. *Cell* **181**, 914-921 e910 (2020).
- 494 5. M. Hoffmann *et al.*, SARS-CoV-2 Cell Entry Depends on ACE2 and TMPRSS2 and Is Blocked by a  
495 Clinically Proven Protease Inhibitor. *Cell* **181**, 271-280 e278 (2020).
- 496 6. R. Yan *et al.*, Structural basis for the recognition of SARS-CoV-2 by full-length human ACE2. *Science*  
497 **367**, 1444-1448 (2020).
- 498 7. D. Wrapp *et al.*, Cryo-EM structure of the 2019-nCoV spike in the prefusion conformation. *Science* **367**,  
499 1260-1263 (2020).
- 500 8. J. Shang *et al.*, Cell entry mechanisms of SARS-CoV-2. *Proc Natl Acad Sci U S A* **117**, 11727-11734  
501 (2020).
- 502 9. A. C. Walls *et al.*, Structure, Function, and Antigenicity of the SARS-CoV-2 Spike Glycoprotein. *Cell* **181**,  
503 281-292 e286 (2020).
- 504 10. C. L. Hsieh *et al.*, Structure-based design of prefusion-stabilized SARS-CoV-2 spikes. *Science* **369**, 1501-  
505 1505 (2020).
- 506 11. S. Bangaru *et al.*, Structural analysis of full-length SARS-CoV-2 spike protein from an advanced vaccine  
507 candidate. *Science* **370**, 1089-1094 (2020).
- 508 12. F. Krammer, SARS-CoV-2 vaccines in development. *Nature* **586**, 516-527 (2020).
- 509 13. A. Mullard, COVID-19 vaccine development pipeline gears up. *Lancet* **395**, 1751-1752 (2020).
- 510 14. Q. Gao *et al.*, Development of an inactivated vaccine candidate for SARS-CoV-2. *Science* **369**, 77-81  
511 (2020).

- 512 15. N. van Doremalen *et al.*, ChAdOx1 nCoV-19 vaccine prevents SARS-CoV-2 pneumonia in rhesus  
513 macaques. *Nature* **586**, 578-582 (2020).
- 514 16. L. Sanchez-Felipe *et al.*, A single-dose live-attenuated YF17D-vectored SARS-CoV-2 vaccine candidate.  
515 *Nature* **590**, 320-325 (2021).
- 516 17. F. C. Zhu *et al.*, Safety, tolerability, and immunogenicity of a recombinant adenovirus type-5 vectored  
517 COVID-19 vaccine: a dose-escalation, open-label, non-randomised, first-in-human trial. *Lancet* **395**, 1845-1854  
518 (2020).
- 519 18. J. Yang *et al.*, A vaccine targeting the RBD of the S protein of SARS-CoV-2 induces protective immunity.  
520 *Nature* **586**, 572-577 (2020).
- 521 19. L. Dai *et al.*, A Universal Design of Betacoronavirus Vaccines against COVID-19, MERS, and SARS. *Cell*  
522 **182**, 722-733 e711 (2020).
- 523 20. J. Yu *et al.*, DNA vaccine protection against SARS-CoV-2 in rhesus macaques. *Science* **369**, 806-811  
524 (2020).
- 525 21. K. S. Corbett *et al.*, SARS-CoV-2 mRNA vaccine design enabled by prototype pathogen preparedness.  
526 *Nature* **586**, 567-571 (2020).
- 527 22. K. S. Corbett *et al.*, Evaluation of the mRNA-1273 Vaccine against SARS-CoV-2 in Nonhuman Primates.  
528 *The New England journal of medicine* **383**, 1544-1555 (2020).
- 529 23. N. N. Zhang *et al.*, A Thermostable mRNA Vaccine against COVID-19. *Cell* **182**, 1271-1283 e1216  
530 (2020).
- 531 24. D. Laczko *et al.*, A Single Immunization with Nucleoside-Modified mRNA Vaccines Elicits Strong  
532 Cellular and Humoral Immune Responses against SARS-CoV-2 in Mice. *Immunity* **53**, 724-732 e727 (2020).
- 533 25. Q. Huang *et al.*, A single-dose mRNA vaccine provides a long-term protection for hACE2 transgenic mice  
534 from SARS-CoV-2. *Nature communications* **12**, 776 (2021).
- 535 26. U. Sahin *et al.*, COVID-19 vaccine BNT162b1 elicits human antibody and TH1 T cell responses. *Nature*  
536 **586**, 594-599 (2020).
- 537 27. A. B. Vogel *et al.*, BNT162b vaccines protect rhesus macaques from SARS-CoV-2. *Nature*, (2021).
- 538 28. N. Pardi, M. J. Hogan, F. W. Porter, D. Weissman, mRNA vaccines - a new era in vaccinology. *Nat Rev*  
539 *Drug Discov* **17**, 261-279 (2018).
- 540 29. N. A. C. Jackson, K. E. Kester, D. Casimiro, S. Gurusathan, F. DeRosa, The promise of mRNA vaccines: a  
541 biotech and industrial perspective. *NPJ Vaccines* **5**, 11 (2020).
- 542 30. M. Durymanov, J. Reineke, Non-viral Delivery of Nucleic Acids: Insight Into Mechanisms of Overcoming  
543 Intracellular Barriers. *Front Pharmacol* **9**, 971 (2018).
- 544 31. O. S. Fenton *et al.*, Bioinspired Alkenyl Amino Alcohol Ionizable Lipid Materials for Highly Potent In  
545 Vivo mRNA Delivery. *Adv Mater* **28**, 2939-2943 (2016).
- 546 32. R. A. Wesselhoeft *et al.*, RNA Circularization Diminishes Immunogenicity and Can Extend Translation  
547 Duration In Vivo. *Mol Cell* **74**, 508-520 e504 (2019).

- 548 33. Y. G. Chen *et al.*, N6-Methyladenosine Modification Controls Circular RNA Immunity. *Mol Cell* **76**, 96-  
549 109 e109 (2019).
- 550 34. X. O. Zhang *et al.*, Complementary sequence-mediated exon circularization. *Cell* **159**, 134-147 (2014).
- 551 35. L. L. Chen, The biogenesis and emerging roles of circular RNAs. *Nat Rev Mol Cell Biol* **17**, 205-211  
552 (2016).
- 553 36. L. S. Kristensen *et al.*, The biogenesis, biology and characterization of circular RNAs. *Nat Rev Genet* **20**,  
554 675-691 (2019).
- 555 37. S. Memczak *et al.*, Circular RNAs are a large class of animal RNAs with regulatory potency. *Nature* **495**,  
556 333-338 (2013).
- 557 38. Y. Euka *et al.*, Circular RNAs are long-lived and display only minimal early alterations in response to a  
558 growth factor. *Nucleic Acids Res* **44**, 1370-1383 (2016).
- 559 39. I. Legnini *et al.*, Circ-ZNF609 Is a Circular RNA that Can Be Translated and Functions in Myogenesis.  
560 *Mol Cell* **66**, 22-37 e29 (2017).
- 561 40. M. Zhang *et al.*, A novel protein encoded by the circular form of the SHPRH gene suppresses glioma  
562 tumorigenesis. *Oncogene* **37**, 1805-1814 (2018).
- 563 41. M. Zhang *et al.*, A peptide encoded by circular form of LINC-PINT suppresses oncogenic transcriptional  
564 elongation in glioblastoma. *Nat Commun* **9**, 4475 (2018).
- 565 42. X. Gao *et al.*, Circular RNA-encoded oncogenic E-cadherin variant promotes glioblastoma tumorigenicity  
566 through activation of EGFR-STAT3 signalling. *Nat Cell Biol*, (2021).
- 567 43. R. A. Wesselhoeft, P. S. Kowalski, D. G. Anderson, Engineering circular RNA for potent and stable  
568 translation in eukaryotic cells. *Nat Commun* **9**, 2629 (2018).
- 569 44. Y. Yang *et al.*, Extensive translation of circular RNAs driven by N(6)-methyladenosine. *Cell Res* **27**, 626-  
570 641 (2017).
- 571 45. Y. Kou *et al.*, Tissue plasminogen activator (tPA) signal sequence enhances immunogenicity of MVA-  
572 based vaccine against tuberculosis. *Immunol Lett* **190**, 51-57 (2017).
- 573 46. J. M. Richner *et al.*, Modified mRNA Vaccines Protect against Zika Virus Infection. *Cell* **169**, 176 (2017).
- 574 47. N. Pardi *et al.*, Zika virus protection by a single low-dose nucleoside-modified mRNA vaccination. *Nature*  
575 **543**, 248-251 (2017).
- 576 48. K. Papanikolopoulou, M. J. van Raaij, A. Mitraki, Creation of hybrid nanorods from sequences of natural  
577 trimeric fibrous proteins using the fibrin trimerization motif. *Methods Mol Biol* **474**, 15-33 (2008).
- 578 49. K. M. Bouwman *et al.*, Multimerization- and glycosylation-dependent receptor binding of SARS-CoV-2  
579 spike proteins. *PLoS Pathog* **17**, e1009282 (2021).
- 580 50. J. W. Fischer, A. K. Leung, CircRNAs: a regulator of cellular stress. *Crit Rev Biochem Mol Biol* **52**, 220-  
581 233 (2017).
- 582 51. X. Ou *et al.*, Characterization of spike glycoprotein of SARS-CoV-2 on virus entry and its immune cross-  
583 reactivity with SARS-CoV. *Nature communications* **11**, 1620 (2020).



- 584 52. C. W. Tan *et al.*, A SARS-CoV-2 surrogate virus neutralization test based on antibody-mediated blockage  
585 of ACE2-spike protein-protein interaction. *Nat Biotechnol* **38**, 1073-1078 (2020).
- 586 53. A. Sette, S. Crotty, Adaptive immunity to SARS-CoV-2 and COVID-19. *Cell* **184**, 861-880 (2021).
- 587 54. Y. Xiang *et al.*, Versatile and multivalent nanobodies efficiently neutralize SARS-CoV-2. *Science* **370**,  
588 1479-1484 (2020).
- 589 55. M. Schoof *et al.*, An ultrapotent synthetic nanobody neutralizes SARS-CoV-2 by stabilizing inactive Spike.  
590 *Science* **370**, 1473-1479 (2020).
- 591 56. T. W. Linsky *et al.*, De novo design of potent and resilient hACE2 decoys to neutralize SARS-CoV-2.  
592 *Science* **370**, 1208-1214 (2020).
- 593 57. A. Muik *et al.*, Neutralization of SARS-CoV-2 lineage B.1.1.7 pseudovirus by BNT162b2 vaccine-elicited  
594 human sera. *Science*, (2021).
- 595 58. Z. Wang *et al.*, mRNA vaccine-elicited antibodies to SARS-CoV-2 and circulating variants. *Nature*,  
596 (2021).
- 597 59. P. Wang *et al.*, Antibody Resistance of SARS-CoV-2 Variants B.1.351 and B.1.1.7. *Nature*, (2021).
- 598 60. W. Tai *et al.*, A novel receptor-binding domain (RBD)-based mRNA vaccine against SARS-CoV-2. *Cell*  
599 *Res* **30**, 932-935 (2020).
- 600 61. Y. Cao *et al.*, Potent Neutralizing Antibodies against SARS-CoV-2 Identified by High-Throughput Single-  
601 Cell Sequencing of Convalescent Patients' B Cells. *Cell* **182**, 73-84 e16 (2020).
- 602 62. S. Du *et al.*, Structurally Resolved SARS-CoV-2 Antibody Shows High Efficacy in Severely Infected  
603 Hamsters and Provides a Potent Cocktail Pairing Strategy. *Cell* **183**, 1013-1023 e1013 (2020).
- 604 63. C. O. Barnes *et al.*, SARS-CoV-2 neutralizing antibody structures inform therapeutic strategies. *Nature*  
605 **588**, 682-687 (2020).
- 606 64. P. A. Koenig *et al.*, Structure-guided multivalent nanobodies block SARS-CoV-2 infection and suppress  
607 mutational escape. *Science* **371**, (2021).
- 608 65. N. G. Davies *et al.*, Increased hazard of death in community-tested cases of SARS-CoV-2 Variant of  
609 Concern 202012/01. *medRxiv*, (2021).
- 610 66. A. S. Luring, E. B. Hodcroft, Genetic Variants of SARS-CoV-2-What Do They Mean? *JAMA* **325**, 529-  
611 531 (2021).
- 612 67. C. K. Wibmer *et al.*, SARS-CoV-2 501Y.V2 escapes neutralization by South African COVID-19 donor  
613 plasma. *Nat Med*, (2021).
- 614 68. K. K. Chan *et al.*, Engineering human ACE2 to optimize binding to the spike protein of SARS coronavirus  
615 2. *Science* **369**, 1261-1265 (2020).
- 616 69. A. Glasgow *et al.*, Engineered ACE2 receptor traps potently neutralize SARS-CoV-2. *Proc Natl Acad Sci*  
617 *USA* **117**, 28046-28055 (2020).
- 618 70. L. M. Ickenstein, P. Garidel, Lipid-based nanoparticle formulations for small molecules and RNA drugs.  
619 *Expert Opin Drug Deliv* **16**, 1205-1226 (2019).



620 71. D. Pinto *et al.*, Cross-neutralization of SARS-CoV-2 by a human monoclonal SARS-CoV antibody. *Nature*  
621 **583**, 290-295 (2020).

622

623

## 624 **ACKNOWLEDGEMENTS**

625 We acknowledge C. Dong and X. Wang (Tsinghua University) for providing fluorescent-  
626 conjugated antibodies. We thank J. Xiao (Peking University) for providing purified SARS-CoV-2  
627 Spike proteins. We thank J. Yan (Institute of Microbiology, Chinese Academy of Sciences) for  
628 providing RBD peptide pools. We thank the Laboratory Animal Centre of Peking University for  
629 the feeding of mice. We thank the HPLC Core at the National Center for Protein Sciences at Peking  
630 University (Beijing), particularly H. Li and G. Li for technical help. We thank the flow cytometry  
631 Core at the National Center for Protein Sciences at Peking University (Beijing), particularly H. Lv,  
632 Y. Guo, H. Yang, F. Wang for technical help.

633

## 634 **Funding:**

635 This project was supported by funds from National Key R&D Program of China  
636 (2020YFA0707800 to W.W., 2020YFA0707600 to Z.Z.); Beijing Municipal Science &  
637 Technology Commission (Z181100001318009); the National Science Foundation of China  
638 (31930016); Beijing Advanced Innovation Center for Genomics at Peking University and the  
639 Peking-Tsinghua Center for Life Sciences (to W.W.); the National Science Foundation of China  
640 (31870893); the National Major Science & Technology Project for Control and Prevention of  
641 Major Infectious Diseases in China (2018ZX10301401 to Z.Z.) and the Fellowship of China  
642 National Postdoctoral Program for Innovative Talents (BX20200010, to L.Q.).

643

## 644 **Author Contributions:**

645 W.W. conceived and supervised this project. W.W., L.Q. and Z.Y. designed the experiments. L.Q.,  
646 Z.Y., Y.S., Y.X., Z.W., H.T., A.Y., and X.X. performed the experiments with the help from Z.Z.,  
647 Y.C., J.W., and X.S.X.. L.Q., Z.Y. and W.W. wrote the manuscript with the help of all other  
648 authors.